Journal of Thermal Science Vol.33, No.2 (2024) 564–577

https://doi.org/10.1007/s11630-024-1860-0 **Article ID: 1003-2169(2024)02-0564-14**

Numerical Investigation on Heat Transfer Characteristics of Microencapsulated Phase Change Material Slurry in a Rectangular Minichannel

WANG Zhibin[1,2], LI Zilong[1,2], JIA Lisi[1,2*], DING Bin[3*], CHEN Ying[1,2]

1. School of Materials and Energy, Guangdong University of Technology, Guangzhou 510006, China
2. Guangdong Provincial Key Laboratory of Functional Soft Condensed Matter, Guangzhou 510006, China
3. College of New Energy, China University of Petroleum (East China), Qingdao 266580, China

Abstract: Microencapsulation phase change material slurry (MEPCMS) becomes a potential working fluid for cooling high energy density miniaturized components, thanks to the latent heat absorption of particles in the heat transfer process. In this work, the Discrete Phase Model (DPM) based on the Euler-Lagrangian method is used to numerically investigate the convective heat transfer characteristics of MEPCMS flowing through a rectangular minichannel with constant heat flux. The results show that particles of MEPCMS are mainly subjected to drag force during the flow. Even so, they can migrate from the high-temperature region to the low-temperature region driven by the thermophoretic force, affecting the particle distribution and phase change process. Moreover, the Nu_x of the MEPCMS fluctuates due to particle phase change with varying specific heat capacities. Specifically, the value increases first, then decreases, and eventually increases again until it approaches the fully developed value of the pure base fluid as the particles gradually melt. Furthermore, the heat transfer performance of the MEPCMS is influenced by the combination of fluid inlet temperature (T_{in}), fluid inlet velocity (v), and mass concentration (c_m) of MEPCM particles. The result shows that the maximum reduction of the maximum bottom wall temperature difference (ΔT_w) is 23.98% at T_{in}=293.15 K, v=0.15 m·s^{-1}, c_m=10%.

Keywords: Microencapsulated Phase Change Material Slurry (MPCMS); Discrete Phase Model (DPM); particle-fluid interaction force; minichannel heat sink; thermophoresis

1. Introduction

In recent years, the performance improvement of communication devices also brings the problem of heat flux increase to electronic components [1–5] with the miniaturization and integration of electronic chips [6]. Ozmat et al. [7] revealed that the reliability of electronic devices is closely related to temperature. For instance, the reliability decreases by 5% when the temperature rises by 1°C within the range of 70°C to 80°C. Statistically, the failure rate of electronic devices induced by high temperatures is 55% [8]. Therefore, effective heat dissipation is essential to keep electronic devices operating safely and stably. Up to now, the mini/microchannel heat sinks [9] are a potential way to cool electronic devices effectively, owing to the advantages of high compactness and large heat transfer specific surface area.

Received: Nov 07, 2022
AE: TANG Guihua

Corresponding author: JIA Lisi; E-mail: jialisi@gdut.edu.cn
DING Bin dingbin@upc.edu.cn

Nomenclature

c_m	particle mass concentrations	T_2	upper melting temperature/K
c_p	specific heat capacity/J·kg^{-1}·K^{-1}	T_{in}	inlet temperature/K
D_h	hydraulic diameter of the channel/mm	v	inlet velocity/m·s^{-1}
d	diameter/mm	y	core-shell weight ratio
H	channel height/mm	**Greek letters**	
h	heat transfer coefficient/W·m^{-2}·K^{-1}	μ	dynamic viscosity/Pa·s
h_{sf}	melting latent heat/kJ·kg^{-1}	ρ	density/kg·m^{-3}
k	thermal conductivity/W·m^{-1}·K^{-1}	**Subscripts**	
L	channel length/mm	c	core
Nu	Nusselt number	f	base fluid
Pr	Prandtl number	p	particle
q	heat flux/W·cm^{-2}	s	shell
Re	Reynolds number	w	wall
T	temperature/K	x	local section of flow direction
T_1	lower melting temperature/K		

However, the conventional coolant (water) becomes unserviceable to satisfy the increasing cooling requirements of electronic devices. Researchers have proved that adding nanoparticles [10, 11] or microencapsulated phase change material (MEPCM) particles [12–14] in cooling water is an effective way to enhance the cooling performance of mini/microchannel heat sinks [15]. Moreover, the MEPCM/water composite coolant is called microencapsulated phase change material slurry (MEPCMS) [16], which can utilize the latent heat absorption capacity of the phase change material during melting. Since then, many studies have been performed on the flow and heat transfer characteristics of MEPCMS from experimental to simulation perspectives. Ho et al. [17] experimentally investigated the convective heat transfer characteristics of MEPCMS in a minichannel heat sink, proving that the cooling performance increased by 51% once MEPCMS replaced the water. Similarly, other experimental results [18–20] indicated that the cooling performance was improved by 52%–170% owing to the difference in flow rate, concentration, materials, etc. However, experimental studies are difficult to reveal the flow heat transfer mechanism, which can be accurately performed by numerical simulation to improve the heat transfer performance further. In the simulation, Zhang et al. [21] performed a 2D numerical analysis of a circular duct with MEPCMS as a coolant. Taking the micro-convection caused by the interaction between the particles and carrier fluid into account, the effective thermal conductivity of the slurry improves. Nevertheless, most of the simulations [22–25] are based on the homogeneous model, which assumes the suspension as a homogeneous fluid with particles uniformly distributed in the base fluid, as well as sets the overall thermophysical parameters during the simulation where different correlations are used by researchers, making it difficult to assess the true performance value of MEPCMS and facilitate its further research.

It is worth mentioning that MEPCMS, as a two-phase fluid, becomes complex in terms of flow and thermal performance compared to conventional single-phase fluid. An interaction exists between the particles and the base fluid, and the particle motion is determined by its force equilibrium. Besides their inertial forces, the particles are subjected to the drag force, lift force, pressure gradient force, virtual mass force, Brownian force, thermophoretic force, etc., exerted by the base fluid (water). The importance of these forces alters in different situations, as in the studies by Buongiorno et al. and Savithiri et al. [26] who found that thermophoretic and Brownian forces can replace inertial force to balance the drag force when the particle size approaches the nanoscale. Therefore, a numerical model that can consider the forces between the two phases is essential. The Discrete Phase Model (DPM) based on the Euler-Lagrangian method treats the base fluid and the particles as continuous and discrete phases, respectively. The model considers the two-phase interaction forces and the particle-wall interaction. It is suitable for simulating two-phase flow and heat transfer phenomena with small volume fractions of discrete phases.

Based on the DPM, Rashidi et al. [27], Shi et al. [28], and Sheikhalipour et al. [29] examined the flow and heat transfer characteristics of nanofluids inside a pipe with an embedded perturbed flow structure and a rectangular microchannel and a trapezoidal microchannel, respectively. Their results showed that the particles were not uniformly distributed. Alquaity et al. [30] and Wu et al. [31] simulated the thermal performance of phase

change particles in different channels and found that DPM can better predict the heat transfer process when comparing the results with the commonly used homogeneous model. However, the above research has not considered the forces comprehensively, and some of them use the equations of thermophoretic coefficient derived for solid-gas mixtures [32] to calculate the thermophoretic force, which may affect the accuracy of particle motion in solid-liquid suspensions and the heat transfer characteristics of the fluid to some extent.

Therefore, it is significant to choose a more realistic two-phase simulation method to simulate the cooling performance of MEPCMS in mini/microchannel. In this work, the convective heat transfer characteristics of MEPCMS in a rectangular minichannel are simulated using DPM. Moreover, to clarify the relationship between particle motion phenomena and the forces on it, the thermophoretic coefficient proposed by Mcnab et al. [33] for solid-liquid mixtures is adopted to correct the thermophoretic force. Furthermore, the effects of particle mass concentration, inlet flow velocity, and inlet temperature on temperature distribution inside the channel, fluid cooling capacity, Nusselt number, and particle phase change behavior are also investigated.

2. Numerical Detail

2.1 Geometry model and boundary conditions

To facilitate the convective heat transfer analysis of MEPCMS, the object targeted in the research is a rectangular channel whose width is much larger than its height. Since the influence of flow and heat transfer in the width direction is ignored, a two-dimensional geometric model can be used as shown in Fig. 1, where the channel has a length L of 1000 mm, a height H of 1 mm, and a characteristic length D_h of 2 mm, which belongs to the category of minichannel [9].

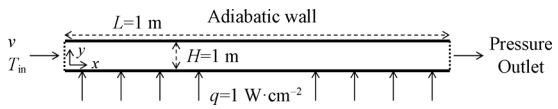

Fig. 1 The schematic representation of the geometric computation model

Boundary conditions are also presented in Fig. 1. The particles following the base fluid are uniformly injected from the inlet with the same velocity v and temperature T_{in} as the base fluid, and zero pressure was specified at the minichannel outlet. Moreover, the top of the channel is an adiabatic wall, and the bottom wall is subjected to a constant heat flux q of 1 W·cm^{-2}. For two-phase flow based on the Euler-Lagrangian method, it is required to consider the particle-wall interaction, also known as the boundary conditions of the particles at the channel boundary, since this interaction may affect the particle concentration distribution. Typically, the particle rebounds off the wall with a change in momentum. The degree of change is determined by the coefficient of restitution, which is the ratio of the velocity after the particle-wall collision to the velocity before the particle-wall collision; meanwhile, it is considered that the particle trajectory tracking stops once the particle reaches the exit. Therefore, the escape boundary condition is used at the entrance and exit of the channel, and the reflect boundary condition with the coefficient of restitution as 1.0 is considered at the channel wall. During the flow of the suspension, MEPCM particles absorb the heat from the bottom, undergo a gradual phase change, and finally outflow from the outlet.

2.2. Thermophysical properties of MEPCMS

In the research, the working fluid is the MEPCMS consisting of MEPCM particles and base fluid (water). Moreover, the shell and core material of the particles is Polymethylmethacrylate (PMMA) and n-Octadecane, respectively. The temperature-dependent relations are used for the thermophysical properties of water (Eqs. (6)–(9)), which are available in heat transfer books and literature [34]. In addition, many researchers [35–37] have evaluated the property parameters of particles from the following equations:

$$y = \frac{m_c}{m_s} \tag{1}$$

$$\rho_p = \frac{(1+y)\rho_c\rho_s}{\rho_s + y\rho_c} \tag{2}$$

$$\left(\frac{d_p}{d_c}\right)^3 = 1 + \frac{\rho_c m_s}{\rho_s m_c} \tag{3}$$

$$\frac{1}{k_p d_p} = \frac{1}{k_c d_c} + \frac{d_p - d_c}{k_s d_p d_c} \tag{4}$$

where y, ρ, d, and k are core-shell weight ratio, density, diameter, and thermal conductivity, respectively. The subscripts c, s, and p represent the core material, shell material, and particle, respectively. It should be noted that the density of the core material is its average density at the solid and liquid states. The diameter of the particle is 5 μm, and the mean mass concentration of the core material (PCM) in an individual MEPCM particle is 80.9%. Since the particles undergo melting, the latent heat of MEPCM particles is reflected by the specific heat capacity, which is regarded as a function of temperature using the effective heat capacity model [36]. For instance, Rao et al. [38] used the same core and shell material to prepare MEPCM particles, and the result of DSC thermal analysis revealed that the specific heat capacity of the obtained particles showed a sinusoidal variation with temperature [37]:

$$c_{p,\mathrm{p}}=\begin{cases}c_{p,\mathrm{c}} & ,\quad T\le T_1\\ c_{p,\mathrm{c}}+\dfrac{\pi}{2}\left(\dfrac{h_{\mathrm{sf}}}{T_{\mathrm{mr}}}-c_{p,\mathrm{c}}\right)\sin\dfrac{(T-T_1)\pi}{T_{\mathrm{mr}}} & ,\quad T_1<T<T_2\\ c_{p,\mathrm{c}} & ,\quad T\ge T_2\end{cases} \tag{5}$$

Table 1 Thermophysical properties of the base fluid and MEPCM

Materials	ρ/kg·m^{-3}	c_p/J·kg^{-1}·K^{-1}	k/W·m^{-1}·K^{-1}	μ/Pa·s	h_{sf}/kJ·kg^{-1}
Water (base fluid)	ρ_{f}	$c_{p,\mathrm{f}}$	k_{f}	μ_{f}	
N-Octadecane (core) solid/liquid state	850/780	2000	0.18	/	241
PMMA (shell)	1180	1440	0.184	/	/
MEPCM	1094		0.1644	/	

The lower melting temperature, upper melting temperature, and melting temperature range of the particles are T_1=297.15 K, T_2=302.15 K, and T_{mr}=5 K, respectively. Thermophysical properties of the base fluid and MEPCM are listed in Table 1.

$$\rho_{\mathrm{f}}=765.33+1.8142T_{\mathrm{f}}-0.0035T_{\mathrm{f}}^2 \tag{6}$$

$$c_{p,\mathrm{f}}=28\,070-281.7T_{\mathrm{f}}+1.25T_{\mathrm{f}}^2-2.48\times10^{-3}T_{\mathrm{f}}^3+8.57\times10^{-6}T_{\mathrm{f}}^4 \tag{7}$$

$$k_{\mathrm{f}}=-0.5752+6.3977\times10^{-3}T_{\mathrm{f}}-8.151\times10^{-6}T_{\mathrm{f}}^2 \tag{8}$$

$$\mu_{\mathrm{f}}=0.0967-8.207\times10^{-4}T_{\mathrm{f}}+2.344\times10^{-6}T_{\mathrm{f}}^2-2.244\times10^{-9}T_{\mathrm{f}}^3 \tag{9}$$

2.3 Model assumptions and governing equations

According to the range of relevant parameters in this study, the following assumptions are made for the convenience of calculation: (1) the suspension can be regarded as a Newtonian fluid due to a low mass concentration (c_{m}<15%) [39]; (2) the flow and heat transfer process is in steady state and incompressible; (3) the thermal radiation and natural convection heat transfer between the wall and the environment are ignored; (4) the suspension in the minichannel is laminar flow due to the low Reynolds number; (5) the gravity and buoyancy are ignored due to similar density between particle and base fluid; (6) the small size particle (d_{p}=5 μm) can be regarded as a homogeneous spherical mass point with internal homogeneous temperature due to low Biot number of the particle [28]; (7) the supercooling phenomenon is ignored due to only considering the melting process of the particle.

To analyze the thermal behavior of the considered suspension, the Discrete Phase Model (DPM) based on the Euler-Lagrangian method is simulated numerically, and the base fluid and particles are treated as the continuous phase and discrete phase, respectively. The gonverning equations for the continuous phase are solved in the Euler coordinate system, and the differential equation of particle motion is integrated into the Lagrangian coordinate system to solve the particle trajectories. The interaction source terms are added to the governing equations to realize the interphase coupling. The conservation of mass, momentum, and energy for the steady incompressible flow of continuous phase is represented as follows [30]:

$$\nabla\cdot\boldsymbol{u}_{\mathbf{f}}=0 \tag{10}$$

$$\nabla\cdot\left(\rho_{\mathrm{f}}\boldsymbol{u}_{\mathbf{f}}\boldsymbol{u}_{\mathbf{f}}\right)=-\nabla p+\mu_{\mathrm{f}}\nabla^2u_{\mathrm{f}}+\boldsymbol{F} \tag{11}$$

$$\nabla\cdot\left[\boldsymbol{u}_{\mathbf{f}}\left(\rho_{\mathrm{f}}E+p\right)\right]=\nabla\cdot\left(k_{\mathrm{f}}\nabla T_{\mathrm{f}}\right)+S \tag{12}$$

where $\boldsymbol{u}_{\mathbf{f}}$, ρ_{f}, μ_{f}, p, k_{f}, and T_{f} are the velocity, density, dynamic viscosity, pressure, thermal conductivity, and temperature of the base fluid, respectively; E is the energy stored by the fluid and can be represented by $E=h_{\mathrm{sf}}-p/\rho_{\mathrm{f}}+u_{\mathrm{f}}^2/2$, where h_{sf} is the apparent enthalpy of the fluid; the source terms $\boldsymbol{F}$ and S in the above equations represent the momentum and energy exchange between the continuous and discrete phases, respectively.

In the Lagrangian coordinate system, the motion equation of a single particle is represented by its force balance as follows [40]:

$$m_{\mathrm{p}}\frac{\mathrm{d}\boldsymbol{u}_{\mathbf{p}}}{\mathrm{d}t}=\boldsymbol{F}_{\mathbf{D}}+\boldsymbol{F}_{\mathbf{other}} \tag{13}$$

$$\boldsymbol{F}_{\mathbf{other}}=\boldsymbol{F}_{\mathbf{V}}+\boldsymbol{F}_{\mathbf{P}}+\boldsymbol{F}_{\mathbf{B}}+\boldsymbol{F}_{\mathbf{T}}+\boldsymbol{F}_{\mathbf{SL}} \tag{14}$$

where m_{p}, $\boldsymbol{u}_{\mathbf{p}}$, t, $\boldsymbol{F}_{\mathbf{D}}$, and $\boldsymbol{F}_{\mathbf{other}}$ are the particle mass, particle velocity, integration time, drag force, and other forces acting on the total mass of the particle, respectively. In this work, other forces include virtual mass force $\boldsymbol{F}_{\mathbf{V}}$, pressure gradient force $\boldsymbol{F}_{\mathbf{P}}$, Brownian force $\boldsymbol{F}_{\mathbf{B}}$, thermophoretic force $\boldsymbol{F}_{\mathbf{T}}$, and Saffman's lift force $\boldsymbol{F}_{\mathbf{SL}}$. These interaction forces are induced by various mechanisms [41–46] and can be calculated as presented in the Appendix.

Furthermore, the energy equation of a single particle is represented by its energy balance as follows [47]:

$$m_{\mathrm{p}}c_{p,\mathrm{p}}\frac{\mathrm{d}T_{\mathrm{p}}}{\mathrm{d}t}=hA_{\mathrm{p}}\left(T_{\mathrm{f}}-T_{\mathrm{p}}\right) \tag{15}$$

where $c_{p,\mathrm{p}}$, T_p, A_p, and h are specific heat capacity, temperature, the surface area of the particle, and fluid-particle heat transfer coefficient at the particle surface, respectively. And h is estimated using the Ranz and Marshall correlation [48]:

$$Nu = \frac{hd_\mathrm{p}}{k_\mathrm{f}} = 2.0 + 0.6Re_\mathrm{p}^{1/2}Pr_\mathrm{f}^{1/3} \tag{16}$$

$$Pr_\mathrm{f} = \frac{c_{\mathrm{p,f}}\mu_\mathrm{f}}{k_\mathrm{f}} \tag{17}$$

$$Re_\mathrm{p} = \frac{\rho_\mathrm{f} d_\mathrm{p} \left|\boldsymbol{u}_\mathbf{p} - \boldsymbol{u}_\mathbf{f}\right|}{\mu_\mathrm{f}} \tag{18}$$

where Pr_f and Re_p are base fluid Prandtl number and particle Reynolds number, respectively. Finally, the momentum transfer and heat transfer in the above continuous phase governing equations are respectively computed by examining the change in momentum and thermal energy of a particle as it passes through each control volume [34]:

$$\boldsymbol{F} = \sum\left[\frac{18\mu_\mathrm{f}}{\rho_\mathrm{p} d_\mathrm{p}^2}\frac{1}{C_\mathrm{C}}\left(\boldsymbol{u}_\mathbf{p} - \boldsymbol{u}_\mathbf{f}\right) + \frac{\boldsymbol{F}_\mathbf{other}}{m_\mathrm{p}}\right]\dot{m}_\mathrm{p}\Delta t \tag{19}$$

$$S = \dot{m}_\mathrm{p} c_{p,\mathrm{p}}\left(T_{\mathrm{p,in-cell}} - T_{\mathrm{p,out-cell}}\right) \tag{20}$$

where $\dot{m}_\mathrm{p}$, $T_{\mathrm{p,in\text{-}cell}}$, and $T_{\mathrm{p,out\text{-}cell}}$ are mass flow rate, temperature at the cell entry and temperature at the cell exit of particle, respectively. Considering the PCM melts inside the capsules, there is no mass exchange, so the particle flow rate in each cell will be conserved. Moreover, the interaction effect between continuous and discrete phases is considered through the momentum and energy exchanges mentioned above.

2.4 Numerical method and validation

In this work, the commercial CFD software FLUENT 2020 R2, based on the finite volume method, is used to convert the governing partial differential equations into algebraic equations. The SIMPLE algorithm solves pressure-velocity coupling, and the convection and pressure terms are discretized by Second order upwind scheme and Standard interpolation scheme, respectively. Furthermore, the Lagrangian particle motion equation is discretized by a modified Euler method.

Moreover, the solving steps of the two-phase flow based on the DPM with two-way coupling method are different from those of the single-phase flow method or the one-way coupling method: firstly, the continuous phase flow field is calculated until partial or complete convergence; then the discrete phase is introduced and the trajectories of each discrete phase injection are calculated; next, the continuous and discrete phases are coupled by source terms in the momentum equation and energy equation, and the continuous phase flow is recalculated; then the discrete phase trajectories are calculated again in the modified continuous phase flow field; finally, the continuous and discrete phase are calculated alternately until the two phases reach the convergence criteria, i.e., in this work the monitored amount of temperature is unchanged with each additional calculation, and the residuals of the continuity, momentum and energy equations are required to be less than 10^{-3}, 10^{-6} and 10^{-8}, respectively. For thermophysical properties of the base fluid and MEPCM mentioned above, codes are developed to describe these using the User Defined Function (UDF) of Fluent.

It should be stated that in DPM, it is not possible to track all physical particles due to the high requirement of computation; instead, representative particles or parcels should be tracked. Any parcel is representative of a specified number of actual particles with the same physical property, where a particle is representative of the entire particles on that parcel, and the motion equation and heat exchange equation are solved only for this particle and extended to others. After solving the equations for the particle, a Gaussian distribution function is used to interpolate the neighboring parcel's impacts on the centroid parcel as follows [49]:

$$\theta_{\mathrm{parcel}} = \sum N_{\mathrm{particle}} G_\omega \theta_{\mathrm{particle}} \tag{21}$$

$$G_\omega = \left(\frac{A}{\pi}\right)^{3/2}\exp\left(-A\frac{\left|x_{\mathrm{parcel}} - x_{\mathrm{particle}}\right|^2}{\Delta x^2}\right) \tag{22}$$

where N_{particle}, G_ω, $\theta_{\mathrm{particle}}$, and θ_{parcel} are the number of particles in the parcel, Gaussian weight function, particle variable in the node, and the accumulation of the particle variable on the node for all parcels, respectively. The variables Δx, x_{parcel}, x_{particle}, and A in the Gaussian weight function are characteristic length scale of the cell, parcel located in the neighborhood, particle location, and a constant of default value 1.0 used to control the width of the Gaussian distribution in this work, respectively. Based on the above equations, the Node-Based Averaging method is provided which distributes the effects of a DPM parcel even into neighboring cells and allows a reduction of grid dependency of DPM simulations.

To certify the sensitivity of the numerical results to the mesh density, a grid independence test was performed at T_in=293.15 K, Re≈392.21, and c_m=10% of MEPCMS. The commercial preprocessor software ICEM CFD 2020 R2 generates a structured rectangular computational mesh across the computational domain. Six grids with increasing fineness, which are 18 348 nodes, 22 011 nodes, 27 511 nodes, 36 685 nodes, 55 011 nodes, and 110 011 nodes, are considered. By comparing the average Nusselt number of various grids, as shown in Table 2, it has been observed that the results do not vary too much for these grids. Specifically, the result of 16 670 grid

numbers almost coincides with that of the 100 000 grid numbers with a relative error of 0.54%, although the difference in the number of the grid between them is about 5 times. Therefore, the grid with a total grid number of 16 670 is selected for the numerical solution with an acceptable compromise between the calculation cost and result accuracy.

Table 2 Grid sensitivity analysis using MEPCMS at T_{in}=293.15 K, Re≈392.21, and c_m=10%

Nodes	Grids	Average Nu	Percentage difference/%
18 348	16 670	6.3202	0.54
22 011	20 000	6.3289	0.40
27 511	25 000	6.3352	0.30
36 685	33 340	6.3397	0.23
55 011	50 000	6.3472	0.11
110 011	100 000	6.3544	/

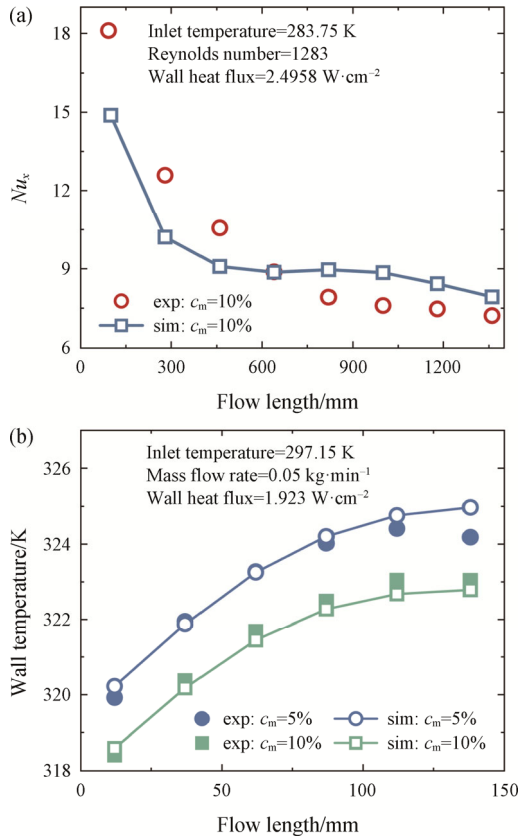

Fig. 2 Comparison of experimental result and simulation data of (a) Zeng et al. [50] and (b) Rao et al. [38] for MEPCMS

Since most experiments mainly focus on macro parameters, it is difficult to find experiments focusing on micro parameters, and the micro level will affect the macro level, so this paper adopts macro parameters to validate the numerical model. And to ensure the reasonability of the numerical method, the model was validated by heat transfer experiments with MEPCMS in different shaped channels since the convective heat transfer mechanism of MECPMS is similar. Zeng et al. [50] studied a circular tube of 1.46-m length and 4-mm inner diameter with a low Reynolds number (laminar flow), the particle diameter of 8.2 μm, and a constant heat flux of 2.4958 W·cm^{-2}. Rao et al. [38] studied a heat sink containing three parallel rectangular minichannels, each of which has 150-mm length, 2-mm width, and 4.2-mm height, with low Reynolds number (laminar flow) and particle diameter of 4.97 μm. Fig. 2(a) shows that the prediction of the local Nusslet number of MEPCMS by DPM simulation is in reasonable agreement with the experimental data [50], and the average relative error is less than 13%. Further, under the operating conditions of the mass flow rate of 0.05 kg·min^{-1} and wall heat flow density of 1.923 W·cm^{-2}, the trend of the wall temperature profiles for both mass concentrations in the simulation is in good agreement with the experimental data [38] with a maximum relative error of 2.9% (as shown in Fig. 2(b)). Hence, the numerical results obtained from DPM in this work are reliable.

3. Results and Discussion

In this section, to fully consider the phase change behavior of the MEPCM particles and keep the Newtonian fluid characteristic of MEPCMS, the simulation results for three factors containing three different levels are discussed, that is, the effects of fluid inlet temperature T_{in} (283.15 K, 288.15 K, and 293.15 K), fluid inlet velocity v (0.10 m·s^{-1}, 0.15 m·s^{-1}, and 0.20 m·s^{-1}), and the mass concentration of the MEPCM particles c_m (5%, 8%, and 10%). Furthermore, the heat transfer performance in terms of temperature field and local Nusselt number Nu_x along the axial direction (x) based on heat transfer coefficient (h_x) is presented, as well as compared with that of water (c_m=0%) under the same operating conditions.

$$T_b = \frac{\sum_{i=1}^{n} T_i \rho_i |\boldsymbol{v}_i \boldsymbol{A}_i|}{\sum_{i=1}^{n} \rho_i |\boldsymbol{v}_i \boldsymbol{A}_i|} \tag{23}$$

$$h_x = \frac{q}{T_w - T_b} \tag{24}$$

$$Nu_x = \frac{h_x D_h}{k_f} = \frac{q D_h}{(T_w - T_b) k_f} \tag{25}$$

The expressions for the related parameters are described above [30], where T_w and T_b are the local bottom wall temperature and local fluid mass-weighted average temperature, respectively. In addition, the effects of the various forces mentioned above and the particle trajectories obtained by DPM on the convective heat transfer characteristics of MEPCMS are also discussed.

3.1. Force analysis of particles in suspension

Understanding the dynamics behaviors of particles in suspension is helpful in accurately describing the heat transfer process of MEPCMS flow. Although various forces act on the particles, only some play dominant roles. Hence, the influence of different forces (i.e., $\boldsymbol{F}_{\mathrm{D}}$, $\boldsymbol{F}_{\mathrm{V}}$, $\boldsymbol{F}_{\mathrm{P}}$, $\boldsymbol{F}_{\mathrm{B}}$, $\boldsymbol{F}_{\mathrm{T}}$, and $\boldsymbol{F}_{\mathrm{SL}}$) on heat transfer can be researched under the characteristics of the DPM approach.

The simulations are carried out at T_{in}=288.15 K, v=0.10 m·s^{-1}, c_{m}=10% for MEPCMS and the results are presented in Fig. 3. All the curves have a high similarity of trend, among which the curve only with drag force is close to the curve with all forces, indicating that the drag force plays a dominant role in MEPCMS flow presented in this work. As investigated by Marshall et al. [44], particle motion is mainly controlled by the force balance between the particle inertial force and the drag force given by the fluid in most particulate flows ignoring collision or external electric, magnetic or gravitational fields. It is worth noting that all curves with a thermophoretic force largely coincide with the trend of the curve with all forces, while only the curve without thermophoretic force largely coincides with the trend of the curve only with the drag force, thus the thermophoretic force has a significant influence on the heat transfer process, especially in the latter part of x. The error of neglecting thermophoretic force is 0.593%, which is much larger than the error (less than 0.05%) of neglecting any other forces (except for drag force). The specific influence mechanism of thermophoretic force on the heat transfer process will be analyzed in combination with the following influencing factors.

3.2 Convective heat transfer characteristics of MEPCMS

To investigate the effects of inlet temperature, inlet velocity and particle mass concentration on the convective heat transfer characteristics of MEPCMS, different combinations of these three parameters were investigated in a comparative method.

Fig. 4 shows the temperature contours of the fluid in the rectangular minichannel under different operating conditions. It can be seen that the overall temperature distribution is wavy along the flowing direction, which stems from the low flow velocity of the fluid near the wall due to the flow boundary layer effect on the one hand, and from the heat originating only from the bottom wall on the other hand. Although the friction in the shear layer contributes to the temperature increase along the length of the channel, the temperature rising inside the channel is mainly the result of external heating. As expected, the heated bottom wall has the highest temperature, and the top adiabatic wall has the lowest temperature at any location along the length of the channel. It is also seen that using MEPCMS as a coolant compared to water results in a more uniform fluid temperature distribution. It indicates that more energy is transferred through the suspension with a low value of coolant temperature increase. It is attributed to the latent heat of melting associated with the phase change of PCM in the particles.

Moreover, increasing the mass concentration of MEPCM particles contributes to a decrease in temperature along the length of the channel, but with different degrees of reduction at different operating conditions. Comparing Fig. 4(a) and 4(b), one can see that the level of the temperature difference between the inlet and outlet temperatures is close for different inlet temperatures. By contrast, the level of temperature difference decreases significantly with increasing inlet velocity when comparing Fig. 4(a) and 4(c). This is because when the heat applied to the whole channel is a constant value, increasing the inlet velocity means increasing the flow rate so that more heat is absorbed per unit of time.

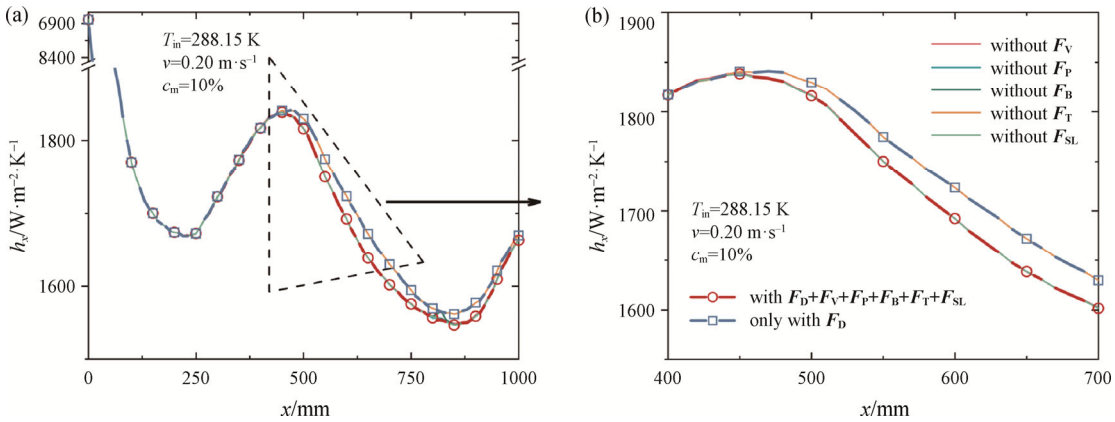

Fig. 3 Local convective heat transfer coefficient in the minichannel for different forces from (a) overall view and (b) partial enlarged view

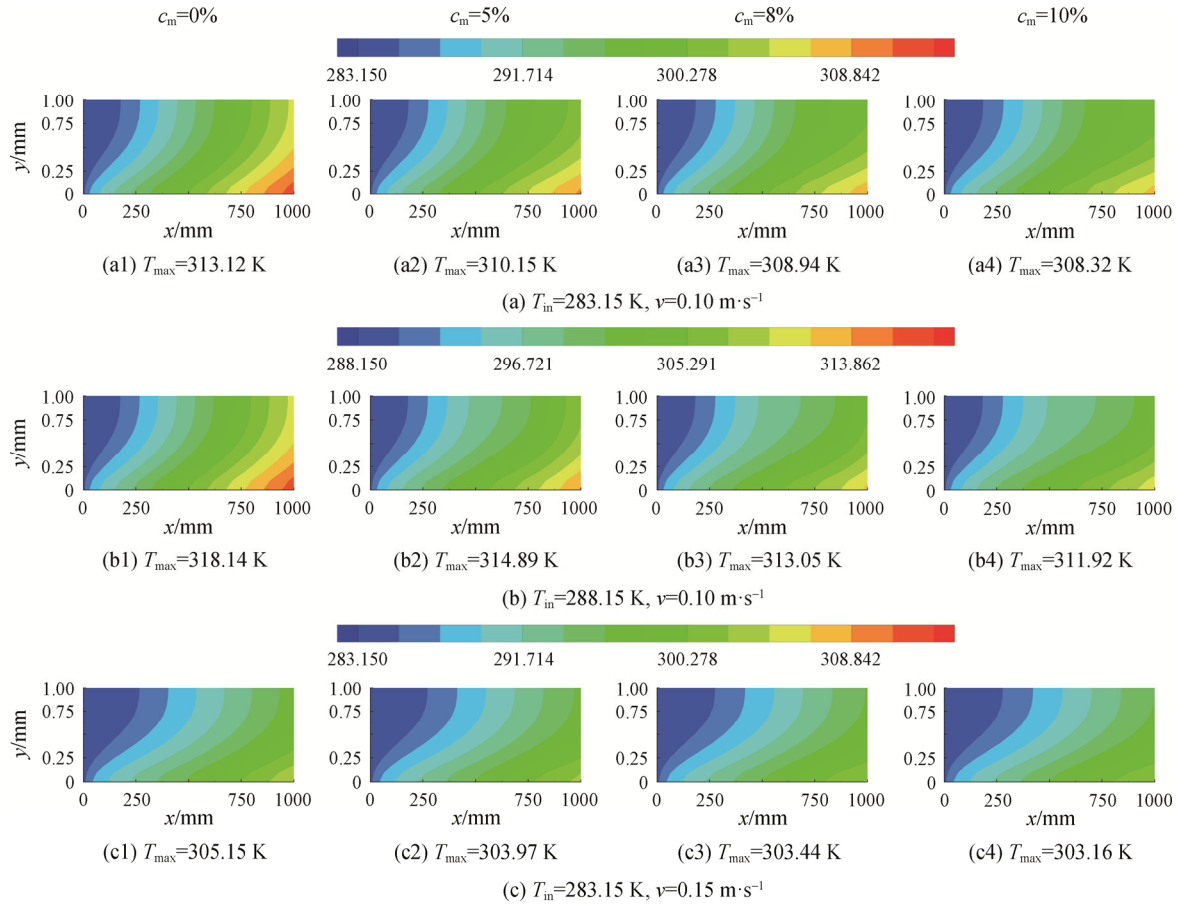

Fig. 4 Temperature contour of fluid inside the minichannel at different operating conditions

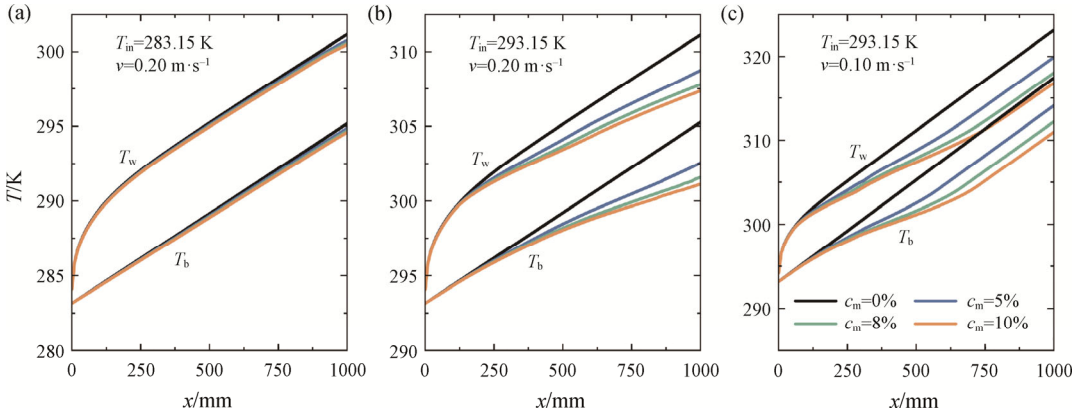

Fig. 5 Temperature of T_w and T_b along minichannel length direction at different operating conditions

While changing only the inlet temperature just affects a small change in the base fluid density so that the fluid flow rate is approximately the same.

Fig. 5 shows the local bottom wall temperature T_w and the local base fluid mass-weighted average temperature T_b in the rectangular minichannel under different operating conditions. It seems clearly that when using pure base fluid as coolant, T_w increases with a gradually decreasing to stable slope in the inlet region, and T_b increases with a stable slope throughout the channel. The slope variation of both temperature curves using the MEPCMS is primarily related to the phase change behavior in the presence of the particles. That is, when the particle temperature is within the melting range, a rapid increase of the equivalent specific heat capacity of the particles due to the latent heat of melting leads to a slowing temperature increase.

It is interesting to note that the melting situation in the calculation region when using the MEPCMS as coolant can be divided into three conditions according to the

slope of the curve. As shown in Fig. 5(a), when suspension with different concentrations flows at T_{in}=283.15 K, v=0.20 m·s^{-1}, both T_w and T_b are slightly lower at the outlet for MEPCMS than those for water. However, the slopes of the curves are close using both suspension and pure water. It indicates that only a small fraction of particles undergo partial melting under these operating conditions. As shown in Fig. 5(b), the temperature difference brought by using MEPCMS can be clearly seen when increasing the inlet temperature to 293.15 K. Since this inlet temperature is close to the particle phase change onset temperature T_1 of 297.15 K, only a shorter distance is needed to attain the particle temperature to T_1 at the given constant heat flux, which in turn allows most of the particles to undergo large portions of melting. Therefore, both the T_w and T_b curves of the suspension occupy a lower slope at large channel distances, which allows the suspension to transport more heat. Comparing Fig. 5(b) and Fig. 5(c), when decreasing the inlet velocity to 0.10 m·s^{-1}, it can be found that the temperature profile of the suspension can be divided into three distinct parts. The fluid outlet temperature increases as the inlet velocity decreases and it reaches a value greater than the particle phase change termination temperature T_2 of 302.15 K. All the particles can complete the phase change process. Then both T_w and T_b curves increase with a large fixed slope. It can also be concluded that within the range considered in this work, the larger the particle mass concentration, the better the cooling effect brought by the suspension, with more heat absorbed by more particles.

Fig. 6 shows the local Nusselt number in the rectangular minichannel for different operating conditions, which is also related to the particle phase change process. As mentioned above, the slope of T_w for pure base fluid decreases until it is close to constant as the fixed slope of T_b. Hence its local Nusselt number decreases in the thermal entrance section until it reaches a fully developed almost constant value. Moreover, the thermal boundary layer thickness decreases as the inlet velocity increases, the greater the distance required for the Nusselt number to reach the thermally fully developed section. As for MEPCMS, the Nusselt number exists fluctuating phenomenon due to the phase change of the particles suspended in the base fluid. Moreover, the fluctuating range is larger for larger particle mass concentrations, including the position of the curve transitions and the magnitude of the curve peak. Under the conditions considered in this work, there are roughly two complete fluctuation profiles of the Nusselt number for water in suspension during the phase change process compared to the pure base fluid: (1) One in which the Nusselt number initially increases and then decreases, and increases again until it reaches almost stability (Fig. 6(a)). (2) The other in which the Nusselt number advances with an approximately fixed value near the inlet, then decreases and increases after reaching a minimum value, and finally reaches a stable value slightly lower than the fully developed value of water (Fig. 6(b)). The second situation of Nu_x is more complex due to the inclusion of the entrance effect, so in this work, the first situation of Nu_x will be explained in connection with the particle trajectories obtained using the DPM.

The operation conditions in Fig. 6(a) are selected and images of the variety of particles' specific heat capacity along the particle trajectories are generated to analyze the Nu_x profile of MEPCMS. The results are shown in Fig. 7 and it indicates that the heat transfer process in the phase change region can be divided by four points. The local bottom wall temperature T_w is greater than the local base fluid mass-weighted average temperature T_b at any axial location as shown in Fig. 5. Moreover, the local Nusselt number Nu_x is a function of the temperature difference between T_w and T_b as indicated by Eq. (25). In the entrance, Nu_x initially decreases as the flow is becoming thermally fully developed as that of the pure base fluid. As the flow develops, the particles near the heated bottom wall begin to melt, which can be seen from the

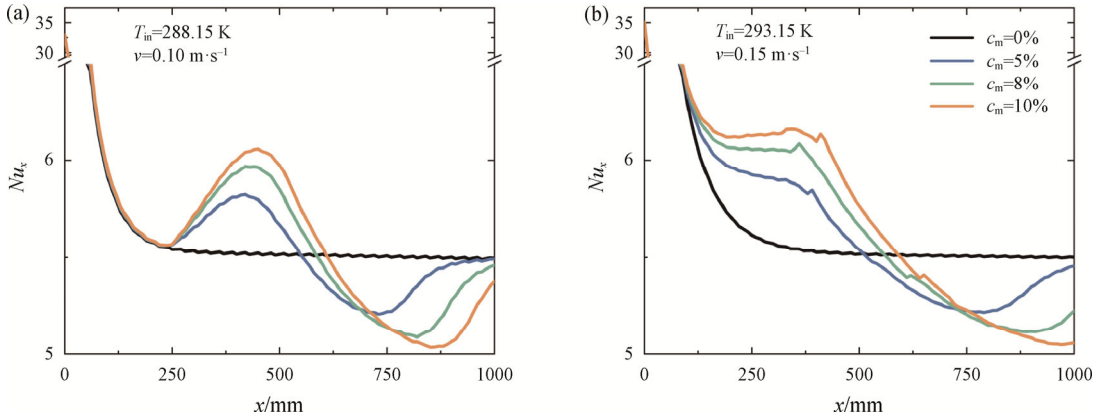

Fig. 6 Local Nusselt number along minichannel length direction at different operating conditions

beginning of the increase in particle-specific heat capacity at point *a*, hence T_w increases slowly. By contrast, T_b increases linearly due to the low value, and as it increases more particles undergo a phase change and the degree of phase change improves, which leads to a decrease in the temperature difference between T_w and T_b, so that Nu_x increases until it reaches a maximum at point *b*. At point *b* the phase change of the particles from the bottom will complete, while the temperature of most particles inside minichannel enters the melting range. Hence T_b increases more slowly than T_w, and the temperature difference becomes larger so that Nu_x decreases until it reaches a minimum value that is smaller than the fully developed Nu_x value of pure base fluid at point *c*. After point *c* most particles complete the phase change, and the increase rate of T_b becomes faster and larger than that of T_w, so Nu_x resumes to increase. It is noteworthy that the particles specific heat capacity of the top trajectory returns to its initial value before the phase change at point *d*, and Nu_x continues to rise. Since only the particles injection from the center of the 10 cells at the inlet of the channel is considered in this work, and the heat only from the bottom causes the highest and lowest base fluid temperature at the same axial position at the bottom and top, respectively. Hence there are still some particles near the top wall, and the rate of heat transfer to the upper right becomes slower, which eventually leads to the phase change process of the particles near point *d** fully completed, and the value of Nu_x is close to that of water.

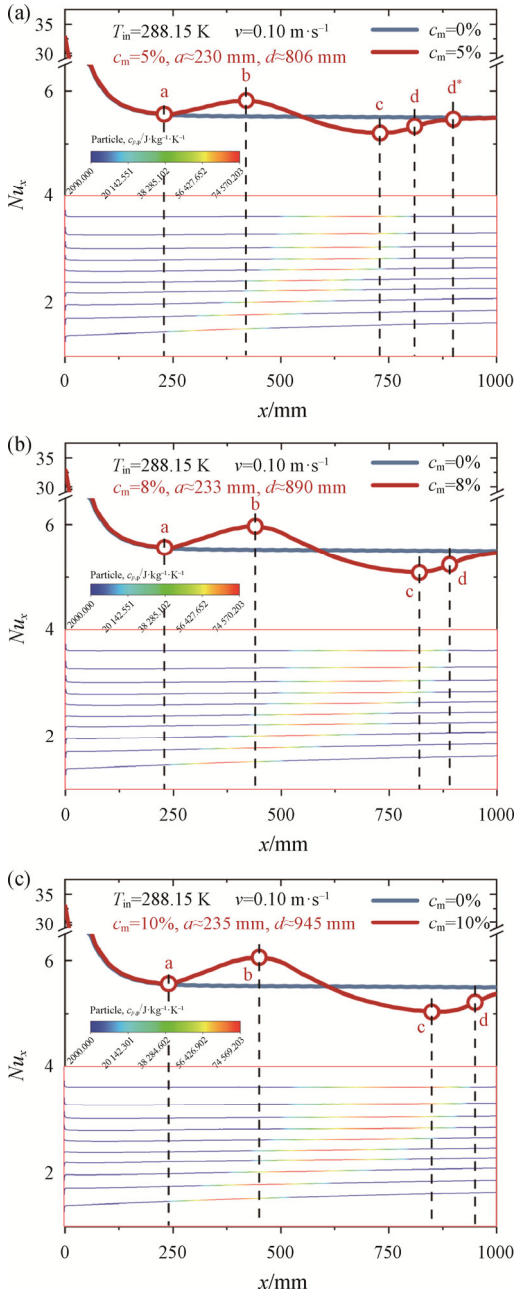

Fig. 7 Local Nusselt number connecting with particle specific heat capacity along the trajectory

Besides, it can be seen that the particles move upward during the flow especially at the bottom, due to the thermophoretic force acting on the particles in the flow field in the direction opposite to the temperature gradient, then causing the particles to migrate form the high-temperature region at the bottom to the low-temperature region at the top. On the one hand, it indicates that the particles suspended in a base fluid are not uniformly distributed as assumed by the homogeneous model. On the other hand, it explains the significant effect of thermophoretic force considered on the local heat transfer coefficient in Fig. 3. For instance, the melting particles deviate from the bottom making T_w increase faster and then causing a larger temperature difference and a decrease in h_x. Furthermore, it can be observed from Figs. 7(a)–(c) that the length of phase change gradually increases from bottom to top and the starting and ending positions of melting lag as the particle mass concentration increases due to the increase in the number of particles represented by each particle trajectory.

3.3. Comprehensive analysis of cooling performance

As discussed above, the value of Nu_x fluctuates above and below the fully developed value of Nu_x for the pure base fluid. Therefore, the local Nusselt number Nu_x is compared to all considered operation conditions as shown in Fig. 8.

From Figs. 8(a)–(c), Figs. 8(d)–(f), and Figs. 8(g)–(i), it can be seen that as the inlet flow velocity increases and the mass flow rate increases, the starting position of particle melting is backward accordingly. It can be deduced that the region of particle melting is also expanded. Increasing the inlet temperature towards the particle phase change onset temperature T_1 of 297.15 K leads to a corresponding forward location of the starting

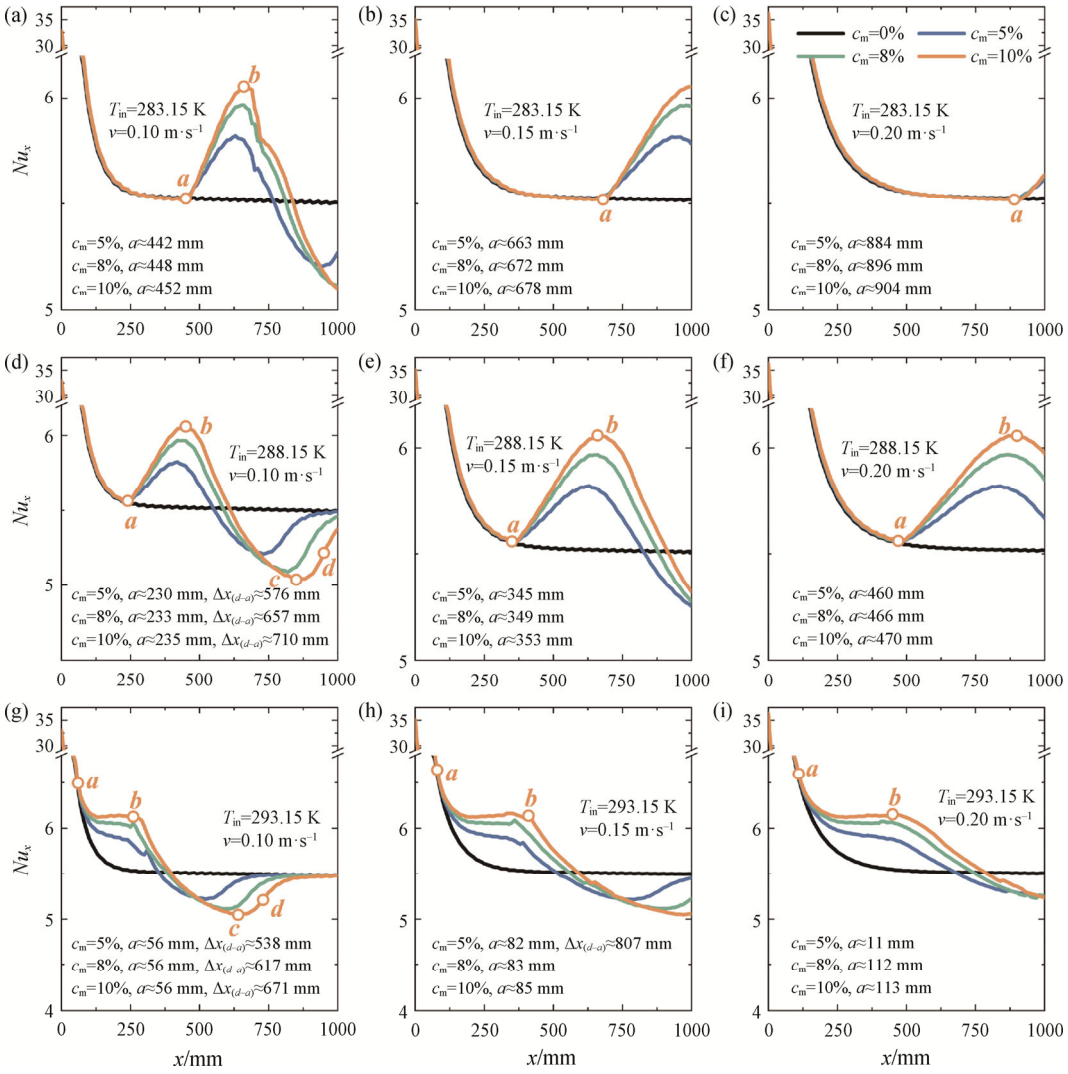

Fig. 8 Local Nusselt number along minichannel length in this work

point of particle melting. Especially, the particle starts the phase change in the entrance section at T_{in}=293.15 K, and the length required to complete the phase change is reduced due to the higher heat transfer rate in the entrance section obtained from Figs. 8(a)-(d)-(g), Figs. 8(b)-(e)-(h), and Figs. 8(c)-(f)-(i). Moreover, the increase in particle mass concentration means that the number of particles inside the channel increases. Hence a longer channel distance is required to facilitate the phase change of the particles and more heat is absorbed by the particles in the form of latent heat over a longer phase change range with a larger peak of Nu_x.

Moreover, the average Nusselt number $\overline{Nu}$ and the maximum bottom wall temperature difference ΔT_w (i.e., the maximum temperature rise in the channel) are calculated as shown in Fig. 9. It can be seen that at the same T_{in}, the $\overline{Nu}$ of the pure base fluid increases linearly in equal proportion with v, while the linearly-increasing $\overline{Nu}$ of the suspension with v is not proportional due to the heat absorption by melting of the particles. Generally, the $\overline{Nu}$ of all considered conditions is close to each other, but at v=0.10 m·s^{-1} and T_{in}=288.15 K, the $\overline{Nu}$ of the pure base fluid can be slightly greater than that of the suspension. Only at high inlet velocity, the $\overline{Nu}$ of the suspension is greater than that of the pure base fluid and the value increases with increasing particle mass concentration. However, the ΔT_w of the suspension is smaller than that of the pure base fluid under all conditions and the value increases with increasing v and c_m. That means the reduction in the bottom wall temperature during the phase change process is mainly attributed to the variable specific heat capacity of the particles rather than to the change of the heat transfer coefficient between the fluid and tube wall. And the

MEPCMS shows a maximum reduction of the ΔT_w by 23.98% at T_{in}=293.15 K, v=0.15 m·s^{-1}, c_m=10% and a maximum improvement of the $\overline{Nu}$ by 3.62% at T_{in}=293.15 K, v=0.20 m·s^{-1}, c_m=10% compared to the pure base fluid. The fluid absorbs heat in the minichannel mainly in the form of the sensible heat capacity of water for the pure base fluid. As for the better cooling effect of the suspension, it can be achieved by the proper matching of the initial working conditions to make the particles fully melt during the flow, so as to make maximum use of the large latent heat capacity of the particles.

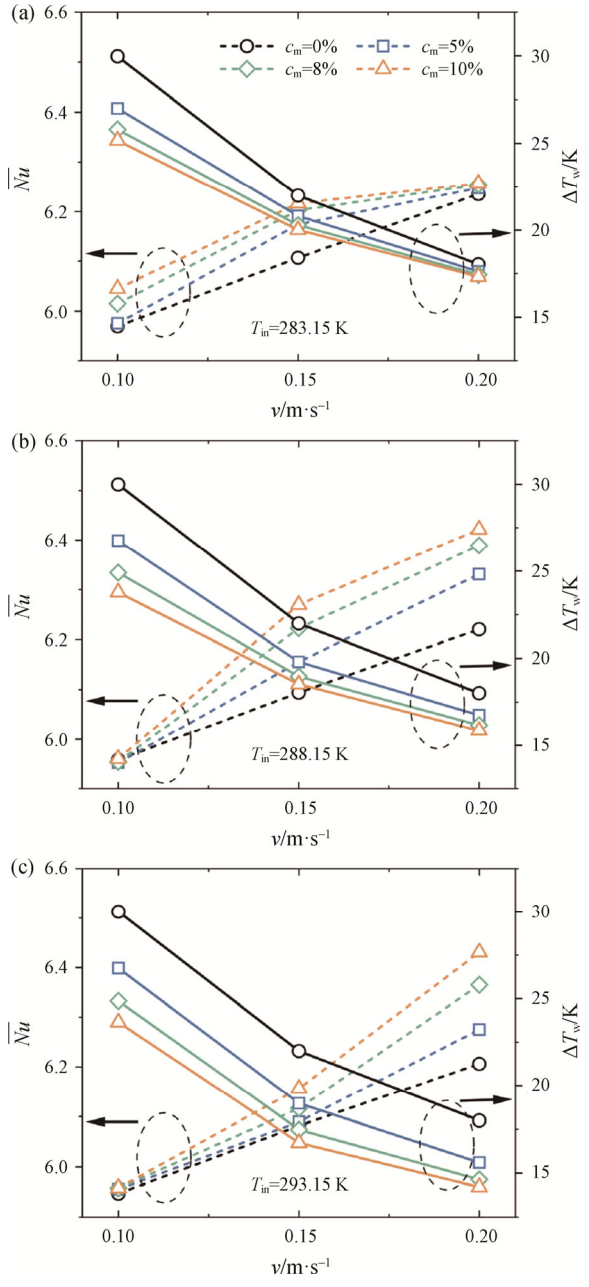

Fig. 9 Average Nusselt number and maximum bottom wall temperature difference in this work

4. Conclusions

In this work, the convective heat transfer characteristics of MEPCMS flowing through a rectangular minichannel with constant heat flux are investigated numerically by using the Discrete Phase Model (DPM) based on the Euler-Lagrangian method, where the forces on the particles in the flow field are taken into account. The conclusions of the numerical simulation with the conditions considered in this work are summarized as follows.

(1) Although the particles of MEPCMS are mainly subjected to drag force during the flow, they can migrate from the high-temperature region to the low-temperature region driven by the thermophoretic force and then affects the particle distribution and phase change process.

(2) The slopes of the temperature curves T_w and T_b both decrease once the particles begin to melt; with the increase of T_{in}, v and c_m, the heat transfer performance of the MEPCMS is improved in different degrees.

(3) The Nu_x of the MEPCMS fluctuates due to particles phase change with varying specific heat capacity; the value increases and then decreases and then increases again until it approaches the fully developed value of the pure base fluid as the particles gradually melt.

(4) The improved heat transfer performance of the MEPCMS compared to the pure base fluid is mainly attributed to the particle phase change behavior, and it shows that the maximum reduction of the ΔT_w is 23.98% at T_{in}=293.15 K, v=0.15 m·s^{-1} and c_m=10%.

Acknowledgments

The authors acknowledge the financial support of the National Natural Science Foundation of China (No. U20A20299), the Natural Science Foundation of Guangdong Province (No. 2019A1515012119).

Conflict of Interest

On behalf of all authors, the corresponding author states that there is no conflict of interest.

Electronic Supplementary Materials

Supplementary materials are available in the online version of this article at

https://doi.org/10.1007/s11630-024-1860-0.

References

[1] Li Y.T., Gong L., Xu M.H., et al., A review of thermo-hydraulic performance of metal foam and its

application as heat sinks for electronics cooling. Journal Electronic Packaging, 2021, 143: 030801.

[2] Bessanane N., Si-Ameur M., Rebay M., Numerical study of the temperature effects on heat transfer coefficient in mini-channel pin-fin heat sink. International Journal of Heat and Technology, 2022, 40: 247–257.

[3] Ding B., Feng W.C., Fang J., et al., How natural convection affect cooling performance of PCM heat sink. International Journal of Heat and Mass Transfer, 2022, 184: 122272.

[4] Zhang Y., Ding B., Zhao D.Y., et al., Effect of natural convection and diffusion on liquid-liquid phase separation behaviors of partially miscible solutions with lower critical solution temperature. International Journal of Heat and Mass Transfer, 2023, 201: 123566.

[5] Ding B., Feng W.C., Mu M.-F., et al., A novel method to concurrently enhance heat conduction and natural convection inside PCM thermal buffer. International Journal of Heat and Mass Transfer, 2023, 203: 123773.

[6] Moore G.E., Cramming more components onto integrated circuits. Proceeding of the IEEE, 1998, 86: 82–85.

[7] Ozmat B., Interconnect technologies and the thermal performance of MCM. IEEE Transactions on Components, Hybrids, and Manufacturing Technology, 1992, 15: 860–869.

[8] Anandan S.S., Ramalingam V., Thermal management of electronics: A review of literature. Thermal Science, 2008, 12: 5–26.

[9] Kandlikar S.G., Grande W.J., Evolution of microchannel flow passages—Thermohydraulic performance and fabrication technology. Heat Transfer Engineering, 2003, 24: 3–17.

[10] Kanti P.K., Sharma K.V., Minea A.A., et al., Experimental and computational determination of heat transfer, entropy generation and pressure drop under turbulent flow in a tube with fly ash-Cu hybrid nanofluid. International Journal Thermal Sciences, 2021, 167: 107016.

[11] Xing M.B., Zhang H.F., Zhang C.C., An update review on performance enhancement of refrigeration systems using nano-fluids. Journal of Thermal Science, 2022, 31: 1236–1251.

[12] Yuan Z.Y., Liang K.F., Xue Y.H., et al., Experimental study of evaluation of dynamical utilization of a microencapsulated phase change material slurry based on temperature range matching analysis. International Communications in Heat and Mass Transfer, 2022, 130: 105788.

[13] Zhang J.J., Yang C.H., Jin Z.G., et al., Experimental study of jet impingement heat transfer with microencapsulated phase change material slurry. Applied Thermal Engineering, 2021, 188: 116588.

[14] Lin Q., Wang S.G., Zhang L., Multi-scale modeling and investigation of thermo-fluidic performance of microencapsulated phase-change material slurry. Journal of Energy Storage, 2021, 37: 102502.

[15] Rehman T.-U., Ambreen T., Niyas H., et al., Experimental investigation on the performance of RT-44HC-nickel foam-based heat sinks for thermal management of electronic gadgets. International Journal of Heat and Mass Transfer, 2022, 188: 122591.

[16] Ghoghaei M.S., Mahmoudian A., Mohammadi O., et al., A review on the applications of micro-/nano-encapsulated phase change material slurry in heat transfer and thermal storage systems. Journal Thermal Analysis and Calorimetry, 2021, 145: 245–268.

[17] Ho C.J., Chen W.C., Yan W.M., Experiment on thermal performance of water-based suspensions of Al_2O_3 nanoparticles and MEPCM particles in a minichannel heat sink. International Journal of Heat and Mass Transfer, 2014, 69: 276–284.

[18] Ho C.J., Chen W.C., Yan W.M., Experimental study on cooling performance of minichannel heat sink using water-based MEPCM particles. International Communications in Heat Mass Transfer, 2013, 48: 67–72.

[19] Wang Y., Chen Z.Q., Ling X., An experimental study of the latent functionally thermal fluid with micro-encapsulated phase change material particles flowing in microchannels. Applied Thermal Engineering, 2016, 105: 209–216.

[20] Chen M., Wang Y., Liu Z.M., Experimental study on micro-encapsulated phase change material slurry flowing in straight and wavy microchannels. Applied Thermal Engineering, 2021, 190: 116841.

[21] Hu X., Zhang Y., Novel insight and numerical analysis of convective heat transfer enhancement with microencapsulated phase change material slurries laminar flow in a circular tube with constant heat flux. International Journal of Heat and Mass Transfer, 2002, 45: 3163–3172.

[22] Seyf H.R., Zhou Z., Ma H.S., et al., Three dimensional numerical study of heat-transfer enhancement by nano-encapsulated phase change material slurry in microtube heat sinks with tangential impingement. International Journal of Heat and Mass Transfer, 2013, 56: 561–573.

[23] Dai H., Chen W., Numerical investigation of heat transfer in the double-layered minichannel with microencapsulated phase change suspension. International Communications in Heat Mass Transfer, 2020, 119: 104918.

[24] Languri E.M., Rokni H.B., Alvarado J., et al., Heat transfer analysis of microencapsulated phase change material slurry flow in heated helical coils: A numerical

and analytical study. International Journal of Heat and Mass Transfer, 2018, 118: 872–878.

[25] Shaukat R., Anwar Z., Imran S., et al., Numerical study of heat transfer characteristics of mPCM slurry during freezing. Arabian Journal for Science and Engineering, 2021, 46: 7977–7988.

[26] Savithiri S., Pattamatta A., Das S.K., Scaling analysis for the investigation of slip mechanisms in nanofluids. Nanoscale Research Letters, 2011, 6: 471.

[27] Rashidi S., Esfahani J.A., Ellahi R., Convective heat transfer and particle motion in an obstructed duct with two side by side obstacles by means of DPM Model. Applied Science-Basel, 2017, 7: 431.

[28] Shi X.J., Li S., Wei Y.D., et al., Numerical investigation of laminar convective heat transfer and pressure drop of water-based Al_2O_3 nanofluids in a microchannel. International Communications in Heat Mass Transfer, 2018, 90: 111–120.

[29] Sheikhalipour T., Abbassi A., Numerical analysis of nanofluid flow inside a trapezoidal microchannel using different approaches. Advanced Powder Technology, 2018, 29: 1749–1757.

[30] Alquaity A.B.S., Al-Dini S.A., Yilbas B.S., Investigation into thermal performance of nanosized phase change material (PCM) in microchannel flow. International Journal Numerical Methods for Heat and Fluid Flow, 2013, 23: 233–247.

[31] Wu X.H., Yang Z., Chen Y., Duan Y.Y., Simulation studies on heat transfer characteristics of PCM micro-encapsulated fluids based on discrete phase model. CIESC Journal, 2020, 71: 1491–1501.

[32] Talbot L., Cheng R.K., Schefer R.W., et al., Thermophoresis of particles in a heated boundary layer. Journal of Fluid Mechanics, 1980, 101: 737–758.

[33] McNAB G.S., MEISEN A., Thermophoresis in liquids. Journal of Colloid and Interface Science, 1973, 44: 339–346.

[34] Mahdavi M., Sharifpur M., Meyer J.P., CFD modelling of heat transfer and pressure drops for nanofluids through vertical tubes in laminar flow by Lagrangian and Eulerian approaches. International Journal of Heat and Mass Transfer, 2015, 88: 803–813.

[35] Ran F.M., Chen Y.K., Cong R.S., et al., Flow and heat transfer characteristics of microencapsulated phase change slurry in thermal energy systems: A review. Renewable and Sustainable Energy Reviews, 2020, 134: 110101.

[36] Yang L., Liu S.L., Zheng H.F., A comprehensive review of hydrodynamic mechanisms and heat transfer characteristics for microencapsulated phase change slurry (MPCS) in circular tube. Renewable and Sustainable Energy Reviews, 2019, 114: 109312.

[37] Chai L., Shaukat R., Wang L., et al., A review on heat transfer and hydrodynamic characteristics of nano/microencapsulated phase change slurry (N/MPCS) in mini/microchannel heat sinks. Applied Thermal Engineering, 2018, 135: 334–349.

[38] Rao Y., Dammel F., Stephan P., et al., Convective heat transfer characteristics of microencapsulated phase change material suspensions in minichannels. Heat and Mass Transfer, 2007, 44: 175–186.

[39] Ran F.M., Xu C.L., Chen Y.K., et al., Numerical flow characteristics of microencapsulated phase change slurry flowing in a helically coiled tube for thermal energy storage. Energy, 2021, 223: 120128.

[40] Mohammadpour J., Lee A., Mozafari M., et al., Evaluation of Al_2O_3-Water nanofluid in a microchannel equipped with a synthetic jet using single-phase and Eulerian-Lagrangian models. International Journal of Thermal Sciences, 2021, 161: 106705.

[41] Ounis H., Ahmadi G., McLaughlin J.B., Brownian diffusion of submicrometer particles in the viscous sublayer. Journal of Colloid and Interface Science, 1991, 143: 266–277.

[42] Das S.K., Choi S.U., Yu W., et al., Nanofluids: science and technology. John Wiley & Sons, 2007.

[43] Mahian O., Kolsi L., Amani M., et al., Recent advances in modeling and simulation of nanofluid flows-Part I: Fundamentals and theory. Physics Reports-Review Section of Physics Letters, 2019, 790: 1–48.

[44] Marshall J., Li S., Adhesive particle flow: A discrete element approach. Cambridge University Press, 2014.

[45] Brown R., XXVII. A brief account of microscopical observations made in the months of June, July and August 1827, on the particles contained in the pollen of plants; and on the general existence of active molecules in organic and inorganic bodies. Philosophical Magazine Series 2, 1828, 4: 161–173.

[46] Michaelides E.E., Wall effects on the Brownian movement, thermophoresis, and deposition of nanoparticles in liquids. Journal of Fluids Engineering, 2016, 138: 051303.

[47] Tahir S., Mital M., Numerical investigation of laminar nanofluid developing flow and heat transfer in a circular channel. Applied Thermal Engineering, 2012, 39: 8–14.

[48] Ranz W.E., Marshall W.R., Evaporation from drops, part I. Chemical Engineering Progress, 1952, 48: 141–146.

[49] Apte S.V., Mahesh K., Lundgren T., Accounting for finite-size effects in simulations of disperse particle-laden flows. International Journal of Multiphase Flow, 2008, 34: 260–271.

[50] Zeng R.L., Wang X., Chen B.J., et al., Heat transfer characteristics of microencapsulated phase change material slurry in laminar flow under constant heat flux. Applied Energy, 2009, 86: 2661–2670.